Geochemical Perspectives Letters



# Physical weathering by glaciers enhances silicon mobilisation and isotopic fractionation

**J.E. Hatton, K.R. Hendry, J.R. Hawkings, J.L. Wadham, L.G. Benning, R. Blukis, V. Roddatis, H.C. Ng, T. Wang.**

## Supplementary Information

The Supplementary Information includes:

- Sample Description
- Detailed Experimental Set-Up
- Agate Mill Tests
- Laboratory Analyses
- Tables S-1 to S-6
- Figures S-1 to S-6
- Supplementary Information References

## Sample Description

Rock debris (ranging from >2 mm finely ground material to up to ~5 cm diameter rock pieces), was collected from the proglacial environment of Leverett Glacier, south-west Greenland, approximately 1 km from the glacier portal (Fig. S-2). Leverett Glacier overlays bedrock that is considered relatively representative of much of the area covered by the Greenland Ice Sheet (GrIS) and once covered by the Fennoscandian ice sheet (Bouysse, 2014; Hawkings *et al.*, 2018). The lithology at Leverett Glacier is dominated by Precambrian Shield granite and gneiss (Lawson *et al.*, 2014). We conducted X-ray diffraction analysis of the samples prior to reaction to assess the mineralogical composition (Fig. S-1), with results showing 47 % albite rich plagioclase, 31 % quartz, 13 % K-feldspar, 6 % Hornblende and 3 % sheet silicates. These results agree well with previous analysis of the area (Hindshaw *et al.*, 2014), thus providing evidence that the material used in these experiments is representative of the region. In addition, Leverett Glacier is one of the most studied outflow glaciers of the GrIS (Bartholomew *et al.*, 2011; Cowton *et al.*, 2012; Clason *et al.*, 2015; Beaton *et al.*, 2017; Hawkings *et al.*, 2017; Kohler *et al.*, 2017; Hawkings *et al.*, 2018), allowing experimental data to be compared to numerous years of field data, helping to contextualise the experimental results.

## Detailed Experimental Set-Up

Proglacial till material collected at Leverett Glacier was briefly rinsed with Ultra-pure water (18.2 MW cm, Milli-Q, Millipore®) and air dried in a laminar flow hood in preparation for crushing. First, rocks were placed in several, thick

polyethene bags and crushed using a sledgehammer and metal plate. The resulting fragments were then passed through mechanical jaws to reduce the particle size further. The sample was then sieved and the <2 mm size fraction was retained for milling. Samples were dry milled using an agate ball mill in a Fritsch Planetary Mono Mill Pulverisette at 500 rpm for either 2 or 30 minutes (T2 and T30), to mimic two different erosion intensities.

After milling, samples were prepared in triplicate for each time point by adding 2.00 ± 0.01 g of milled sediment to 50 mL centrifuge tubes, cleaned by soaking in 2M HCl for 24 hours then ultra-pure (MQ) water for 24 hours. Experiments were started with the addition of 40 mL MQ water to the milled rock material. A sediment: water ratio of 50 g $L^{-1}$ was used in all dissolution experiments, as this is sufficiently high to mimic rock-water ratios in the subglacial environment, when considering the potentially high erosion rates calculated from suspended sediment fluxes at LG. Samples were kept at 4 °C on a shaker at 100 rpm in the dark for the duration of the experiment. At pre-determined timepoints (4, 24, 48, 168, 336 and 720 hours) experiments were terminated by centrifuging the tubes and filtering the supernatant through 0.22 µm Sartorius™ Minisart™ High Flow PES membrane filters. The filtrate was stored at 4 °C until analysis and the sediments were allowed to air dry in a laminar flow hood (IS05). Once dry, the sediment was partitioned for solid state analysis or re-crushing. Re-crushing was completed using a pestle and mortar and the experiment outlined above was repeated by reacting the solids for 4, 48 and 720 hours again with MQ water.

Control experiments were set up to establish DSi and ASi concentrations of starting material prior to milling. Here, unmilled material was added to centrifuge tubes and then 40ml of MQ water was added. The control experiments were kept under the same conditions as the milled experiments, as outlined above. However, it was not possible to keep the sample weight of the control experiments at 2.00 ± 0.01 g, due to the large size of some un-milled material. Despite the greater sediment to water ratios, Table S-5 shows that DSi concentrations from unmilled samples were <3 % of the total DSi content from milled experiments. These values have been blanked corrected using an average for the full experimental blank (0.33 µM, n = 3), where MQ water was added to cleaned centrifuge tubes and left on a shaker at 4 °C for 720 hours. Control ASi concentrations were calculated from unmilled starting material that was either unreacted with MQ water or reacted with MQ water for up to 168 hours (from the DSi control experiments). ASi extractions were completed using the same methodology as outlined below, with a weak alkaline leach for up to 5 hours. Table S-6 shows that the ASi extracted from unmilled starting material is <7 % of the T2 experiment sets and <2 % of the T30 experiment sets. The range of ASi concentrations from the control experiments (below limit of detection to 0.04 wt. %) highlights the heterogenous nature of the starting material, with larger rocks (with a smaller specific surface area) resulting in the lowest ASi concentrations.

## Agate Mill Tests

The milling methodology employed follows procedures routinely carried out in the silicon isotope community (*i.e.* to establish bulk Si isotopic composition of solid materials) and previous testing has been conducted to show that agate ball milling does not result in any sample contamination with respect to Si (Savage *et al.*, 2011). However, we recognise that previous tests did not mill material for 30 minutes, so we completed some additional tests to ensure this increased milling did not result in any contamination from the agate ball mill.

Samples were milled in a Retsch Mixer Mill MM 400, using both steel and agate mills for up to 30 minutes (stopping at 2, 4, 10, 20 and 30 minutes to collect sub-samples for analysis). Samples were milled at 8.33 Hz and each sub-sample was mixed with 10 wt. % $CeO_2$ before XRD analysis. This allowed us to compare any differences in ASi concentration between the agate and steel mills and assess any potential contamination. Figure S-6 shows no significant differences in ASi concentrations for all timepoints between the steel and agate mills, during XRD analysis.

# Laboratory Analyses

Water samples were stored refrigerated prior to analysis for major ion concentrations, DSi concentrations and $\delta^{30}Si_{DSi}$. Major ion concentrations were analysed by capillary ion chromatography using a Thermo Scientific Dionex ICS-5000+, as described previously by Hawkings *et al.* (2015). DSi concentrations were analysed spectrophotometrically using Flow Injection Analysis, as described by Hatton *et al.* (2019) and Hawkings *et al.* (2018).

Once dry, the solid phase was partitioned for alkaline extraction to determine ASi concentration. ASi concentrations were determined using an alkaline 0.1 M $Na_2CO_3$ extraction, modified from Demaster (1981) and used previously for riverine suspended sediments (Hatton *et al.*, 2019).

### Silicon Isotope Composition

Samples were measured for dissolved, amorphous and bulk ($\delta^{30}Si_{DSi}$, $\delta^{30}Si_{ASi}$, and $\delta^{30}Si_{bulk}$ respectively) silicon isotope composition using a Thermo Scientific Neptune Plus High-Resolution MC-IPC-MS in the Bristol Isotope Group Laboratories at the University of Bristol. Methods are detailed previously in Hatton *et al*. (2019) and Hawkings *et al.* (2018). Briefly, measurements of $^{28}Si$, $^{29}Si$ and $^{30}Si$ were made in triplicate in wet plasma mode. Standard-sample-standard bracketing was employed and all samples and standards were doped with 100 µL of 10 ppm Mg solution to correct for instrumental mass bias (Cardinal *et al*., 2010) and 50 µL $H_2SO_4$ (0.01 M) to remove any anionic mass bias matrix effects (Hughes *et al*., 2011). Results are reported as $\delta^{30}Si$, which is calculated based on the deviation from the ratio of $^{28}Si/^{30}Si$ from the bracketing standard:

$$\delta^{30}Si = \left[\frac{\left(\frac{^{30}Si}{^{28}Si}\right)sample}{\left(\frac{^{30}Si}{^{28}Si}\right)NBS28} - 1\right] x\ 1000 \qquad \text{Eq. S-1}$$

A three isotope plot (Fig. S-6) demonstrates that samples and standards measured for this study display mass dependent fractionation, with a gradient of 0.5119 (Reynolds *et al.*, 2007). Reference standards LMG ($\delta^{30}Si$ = -3.42 ± 0.13 ‰, 2 s.d., n = 13) and Diatomite ($\delta^{30}Si$ = +1.22 ± 0.14 ‰, 2 s.d., n = 24) measured alongside samples show good agreement with published values (Reynolds *et al.*, 2007; Hendry *et al.*, 2011). Long term reproducibility of these standards measured between 2015–2020 also show good agreement with published values (LMG: -3.44 ± 0.07 ‰ 2 s.d., n = 138; Diatomite: +1.22 ± 0.07 ‰, 2 s.d., n = 99).

### Grainsize Analysis

Grain size was measured using a Malvern Mastersizer 3000 system, that can measure particle sizes between 0.02 µm and 2000 µm. Ultra pure Milli-Q water was used as the dispersion media and an obscurity between 5–15 % (stability ± 0.1 %) was ensured. Internal precision (average 2 s.d. = 1.2 %) was calculated from five measurements of each sample and selected samples were replicated in triplicate to assess external reproducibility (average 2 s.d. = 7 %). Analysis showed that re-crushing the solid phase using a pestle and mortar resulted in consistent grainsize distributions within the T2 and T30 samples.

### High resolution transmission electron microscopy (HR-TEM)

Initial, milled and reacted samples were imaged and spectrally analysed using a high-resolution transmission electron microscope (HR-TEM, FEI Tecnai TF20 at 200 kV). A small amount of sample (<10 mg) was dispersed for 10 minutes in ethanol in a microcentrifuge tube using an ultrasonic bath. A 2–4 µL drop of the

dispersed solution was pipetted onto a holey carbon support grid and allowed to dry. Images and analyses were collected on a TECNAI F20 XTWIN TEM operated at 200 kV with a field emission gun electron source, a Gatan Imaging Filter (GIF) Tridiem™, and an EDAX X-ray analyser.

**X-Ray Scattering Analysis**

***Reduced pair distribution function (G(r)) analysis.*** The changes induced due to the milling and reaction with water were analysed using G(r) analysis calculated from measured total X-ray scattering patterns. For these measurements the powdered samples where loaded in 0.5 mm diameter glass capillaries (Hilgenberg 4007405). X-ray scattering patterns were measured using a STOE STADI P instrument with an Ag X-ray source ($\lambda$ = 0.55941 Å), curved Ge (111) monochromator and DECTRIS MYTHEN2 detector. Measurements were performed in a Debye-Scherrer geometry for a Q up to 20.52 $Å^{-1}$ and with an angular resolution of 0.015°. Average measurement time per sample was 4 days with longer measurement time scaled for the high Q regions. The scattering data was processed using PDFgetX2 software (Qiu *et al.*, 2004). The raw X-ray scattering pattern was corrected for sample geometry, capillary and air scattering background, absorption, radiation polarisation, Compton scattering and multiple (2nd) scattering to obtain the correct structure factor S(Q) (Egami and Billinge, 2003). For absorption and atomic form factor corrections, we also determined the average chemical composition of the samples (64 at. % O, 21 at. % Si, 7 at. % Al, 4 at. % Na, 2 at. % K, 1 at. % Ca, 0.7 at. % Fe, 0.4 at. % Mg, 0.2 at. % Ti; ±5 at. % error can be assumed for all elements) using a scanning electron microscope (FEI Quanta 3D, run at 20 keV) equipped with an EDAX EDS detector (EDAX Loctane ELECT PLUS). In all cases a large area of the sample was mapped to determine elemental contributions, and the composition was then assumed to be the same across the whole sample.

***Mineralogical analysis.*** Mineralogical changes and amorphous content of the samples was measured from diffractions patterns measured using a STOE STADI P instrument with a Cu X-ray source ($\lambda$ = 1.5406 Å), curved Ge (111) monochromator and DECTRIS MYTHEN2 detector in Debye-Scherrer geometry. The powdered samples were mixed with approximately 10 wt. % of precisely measured amount of $CeO_2$ and loaded in 0.5 mm diameter glass capillaries (Hilgenberg 4007405). The scattering pattern was measured in range of 0–84° 2$\theta$ with a resolution of 0.015° and the measurement time of 6 hours per sample (10,700 seconds per degree 2$\theta$). The instrument profile was calibrated using a NIST Si standard. For Rietveld analysis mineral reference CIF files were obtained from COD database. The background was fitted with an empirical polynomial function. The mineral cell parameters, grain size, microstrain and solid solution composition, where appropriate, were allowed to vary during the refinement. The accuracy of the refinement is estimated to be within 2–5 wt. %.

# Supplementary Tables

**Table S-1** Summary of results from original batch experiments. Each batch included 3 replicate samples, with the standard deviation between these samples shown in square brackets (where available). Isotopic external error is the variability in triplicate measurements of a single sample (2 s.d.).

| Batch | Milling Time (mins) | Incubation Time (hours) | DSi (µM) [s.d., n = 3] | $\delta^{30}Si_{DSi}$ (‰) [s.d., n = 3] | $\delta^{30}Si_{DSi}$ Ext. error (‰), 2 s.d., n = 3 | ASi (%) [s.d., n = 3] | $\delta^{30}Si_{ASi}$ (‰) | $\delta^{30}Si_{ASi}$ Ext. error (‰) 2 s.d., n = 3 | Divalent: Monovalent (D:M) Ion ratio (µM) [s.d., n = 3] |
|---|---|---|---|---|---|---|---|---|---|
| T2-4 | 2 | 4 | 13.04 [0.77] | -1.97 [0.17] | 0.04 | 0.08 [0.02] | -0.18 | 0.09 | 0.13 [0.01] |
| T2-24 | 2 | 24 | 18.58 [0.86] | -0.95 | 0.13 | 0.10 | -0.20 | 0.08 | 0.09 [0.01] |
| T2-48 | 2 | 48 | 31.49 [0.22] | -0.80 | 0.09 | 0.30 [0.13] | -0.24 | 0.05 | 0.12 [0.01] |
| T2-120 | 2 | 120 | 24.70 [2.81] | -0.48 | 0.12 | 0.10 | -0.25 | 0.08 | 0.12 [0.01] |
| T2-336 | 2 | 336 | 31.49 [1.03] | -0.98 [0.08] | 0.08 | 0.15 | -0.29 | 0.01 | 0.12 [0.01] |
| T2-720 | 2 | 720 | 51.17 [4.29] | -0.13 | 0.15 | 0.05 | -0.15 | 0.10 | 0.16 [0.01] |
| T30-4 | 30 | 4 | 46.13 [2.23] | -1.56 | 0.09 | 0.67 | -0.17 | 0.02 | 0.03 [<0.01] |
| T30-24 | 30 | 24 | 57.61 [0.97] | -0.62 | 0.04 | 0.53 [0.11] | -0.12 | 0.02 | 0.02 [<0.01] |
| T30-48 | 30 | 48 | 58.06 [1.21] | -0.53 [0.02] | 0.06 | 0.48 | -0.10 | 0.11 | 0.03 [<0.01] |
| T30-120 | 30 | 120 | 73.47 [2.25] | -0.33 | 0.01 | 0.98 [0.09] | -0.23 | 0.03 | 0.03 [<0.01] |
| T30-336 | 30 | 336 | 89.01 [3.38] | -0.71 [0.03] | 0.07 | 1.45 | -0.24 | 0.09 | 0.02 [<0.01] |
| T30-720 | 30 | 720 | 81.12 [5.28] | -0.07 | 0.01 | 0.62 [0.13] | -0.21 | 0.09 | 0.04 [<0.01] |

**Table S-2** Summary of results from batch experiments after re-crushing. Each batch included triplicate samples, with the standard deviation between these samples shown in square brackets.

| Batch | Original Milling Time (mins) | Secondary Incubation Time (hours) | Average DSi (µM) [s.d., n = 3] | $\delta^{30}Si_{DSi}$ (‰) [s.d., n = 3] | ASi (%) [s.d., n = 3] | $\delta^{30}Si_{ASi}$ (‰) [s.d., n = 3] | Average D:M (µM) [s.d., n = 3] |
|---|---|---|---|---|---|---|---|
| T2-RC4 | 2 | 4 | 11.06 [1.34] | -1.14 [0.12] | 0.15 [0.02] | -0.25 [0.02] | 0.04 [0.03] |
| T2-RC48 | 2 | 48 | 21.62 [1.01] | -1.05 [0.05] | 0.08 [0.05] | -0.16 [0.02] | 0.02 [0.01] |
| T2-RC720 | 2 | 720 | 49.51 [2.25] | -0.17 [0.06] | 0.21 [0.04] | -0.30 [0.02] | 0.08 [0.05] |
| T30-RC4 | 30 | 4 | 25.25 [2.15] | -0.99 [0.12] | 0.98 [0.02] | -0.19 [0.08] | 0.01 [<0.01] |
| T30-RC48 | 30 | 48 | 48.99 [2.33] | -0.59 [0.10] | 0.95 [0.04] | -0.22 [0.06] | <0.01 [<0.01] |
| T30-RC720 | 30 | 720 | 89.01 [3.10] | -0.01 [0.03] | 0.66 [0.28] | -0.22 [0.07] | 0.01 [<0.01] |

**Table S-3** Molar major ion concentrations from batch experiments. Each batch included triplicate samples, with the standard deviation between these samples shown in square brackets.

| Batch | Milling Time (mins) | Incubation Time (hrs) | Average $Ca^{2+}$ (µM) [s.d., n = 3] | Average $Mg^{2+}$ (µM) [s.d., n = 3] | Average $Na^{+}$ (µM) [s.d., n = 3] | Average $K^{+}$ (µM) [s.d., n = 3] | Divalent: Monovalent (D:M) Ion ratio (µM) [s.d., n = 3] |
|---|---|---|---|---|---|---|---|
| T2-4 | 2 | 4 | 4.33 [1.06] | 8.85 [1.49] | 71.67 [10.51] | 40.36 [6.85] | 0.13 [0.01] |
| T2-24 | 2 | 24 | 3.94 [0.62] | 7.09 [0.38] | 75.40 [3.41] | 52.35 [1.38] | 0.09 [0.01] |
| T2-48 | 2 | 48 | 6.91 [1.88] | 9.02 [0.62] | 77.92 [0.07] | 55.11 [0.19] | 0.12 [0.01] |
| T2-120 | 2 | 120 | 6.11 [1.00] | 9.64 [0.91] | 87.63 [4.42] | 53.51 [7.53] | 0.12 [0.01] |
| T2-336 | 2 | 336 | 5.23 [0.62] | 11.33 [2.30] | 107.29 [0.12] | 55.62 [0.89] | 0.12 [0.01] |
| T2-720 | 2 | 720 | 12.73 [1.51] | 17.66 [2.71] | 113.45 [7.04] | 78.50 [4.57] | 0.16 [0.01] |
| T30-4 | 30 | 4 | 384.27 [11.92] | 206.85 [6.66] | 13.11 [0.822] | 2.13 [0.52] | 0.03 [<0.01] |
| T30-24 | 30 | 24 | 334.21 [5.13] | 172.32 [1.71] | 9.83 [0.99] | 1.50 [0.37] | 0.02 [<0.01] |
| T30-48 | 30 | 48 | 340.89 [4.99] | 173.32 [1.71] | 11.60 [0.34] | 2.42 [0.26] | 0.03 [<0.01] |
| T30-120 | 30 | 120 | 401.05 [13.05] | 192.98 [7.22] | 13.02 [0.48] | 3.02 [0.29] | 0.03 [<0.01] |
| T30-336 | 30 | 336 | 548.41 [12.45] | 238.69 [11.03] | 11.72 [1.08] | 1.07 [1.27] | 0.02 [<0.01] |
| T30-720 | 30 | 720 | 514.89 [6.86] | 223.84 [5.70] | 14.84 [1.95] | 3.35 [0.80] | 0.04 [<0.01] |

**Table S-4** Molar major ion concentrations from batch experiments. Each batch included triplicate samples, with the standard deviation between these samples shown in square brackets.

| Batch | Original Milling Time (mins) | Secondary Incubation Time (hours) | Average $Ca^{2+}$ (µM) [s.d., n = 3] | Average $Mg^{2+}$ (µM) [s.d., n = 3] | Average $Na^{+}$ (µM) [s.d., n = 3] | Average $K^{+}$ (µM) [s.d., n = 3] | Average D:M (µM) [s.d., n = 3] |
|---|---|---|---|---|---|---|---|
| T2-RC4 | 2 | 4 | 1.82 [1.61] | 2.87 [1.53] | 77.13 [4.67] | 44.37 [6.28] | 0.04 [0.03] |
| T2-RC48 | 2 | 48 | 0.64 [0.45] | 2.52 [2.25] | 79.19 [11.35] | 39.78 [1.07] | 0.02 [0.01] |
| T2-RC720 | 2 | 720 | 4.35 [3.62] | 7.07 [4.64] | 103.89 [20.59] | 52.48 [6.27] | 0.08 [0.05] |
| T30-RC4 | 30 | 4 | 0.34 [0.25] | 1.19 [0.37] | 220.15 [21.63] | 69.97 [13.61] | 0.01 [<0.01] |
| T30-RC48 | 30 | 48 | <LOD | 1.37 [0.81] | 281.36 [49.38] | 85.96 [6.34] | <0.01 [<0.01] |
| T30-RC720 | 30 | 720 | <LOD | 2.03 [0.47] | 262.58 [19.03] | 99.25 [8.61] | 0.01 [<0.01] |

**Table S-5** Summary of DSi concentrations results from unmilled control experiments. <LoD = Below Limit of Detection (FIA LoD = 10 ppb). Unmilled rock debris was reacted with MQ-grade water for 4, 24, 48 and 168 hours.

| Sample | Incubation Time (hrs) | Average DSi (µM) (n = 3) | DSi (µM) range | Total of [DSi] measured from T2 experiments at same timepoint (%) | Total of [DSi] measured from T2 experiments at same timepoint (%) |
|---|---|---|---|---|---|
| Unmilled Control – 4 | 4 | 0.09 | 0.08–0.12 | 0.71 | 0.20 |
| Unmilled Control -24 | 24 | 0.25 | 0.15–0.43 | 1.30 | 0.43 |
| Unmilled Control -48 | 48 | 0.44 | 0.18–0.88 | 2.36 | 0.75 |
| Unmilled Control - 168 | 168 | 0.58 | 0.46–0.77 | 2.37 | 0.80 |

**Table S-6** Summary of ASi concentrations results from unmilled control experiments. ASi concentrations measured after $Na_2CO_3$ extraction of unmilled rock samples. <LoD = Below Limit of Detection (FIA LoD = 10 ppb).

| Sample | Incubation Time (hrs) | Sample weight (g) | ASi (wt. %) |
|---|---|---|---|
| ASi Control 1 | Unreacted | 0.32 | 0.014 |
| ASi Control 2 | Unreacted | 11.44 | 0.002 |
| ASi Control 3 | Unreacted | 3.78 | 0.004 |
| ASi Control 4 | Unreacted | 0.51 | 0.022 |
| ASi Control 5 | 4 | 7.90 | 0.001 |
| ASi Control 6 | 24 | 0.71 | 0.010 |
| ASi Control 7 | 48 | 0.16 | 0.035 |
| ASi Control 8 | 168 | 0.50 | <LOD |
| Average | - | - | 0.011 |
| Total of [ASi] measured from T2 (%) | - | - | 6.41 |
| Total of [ASi] measured from T30 (%) | - | - | 1.68 |

# Supplementary Figures

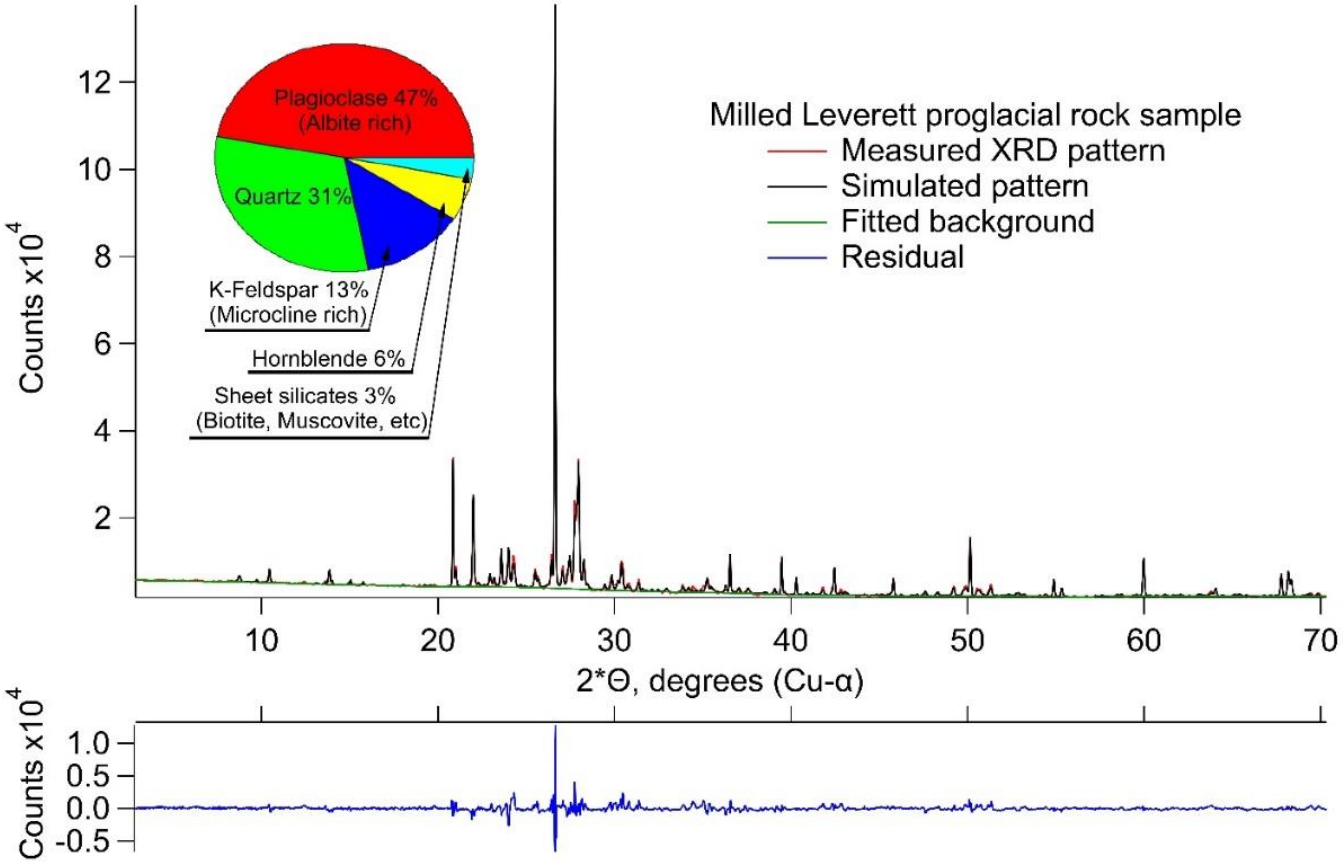


**Figure S-1** Mineral composition of proglacial rock debris derived from X-ray diffraction analyses. Shown are measured and Rietveld refined, simulated patterns as well as residual (see y-axis difference).

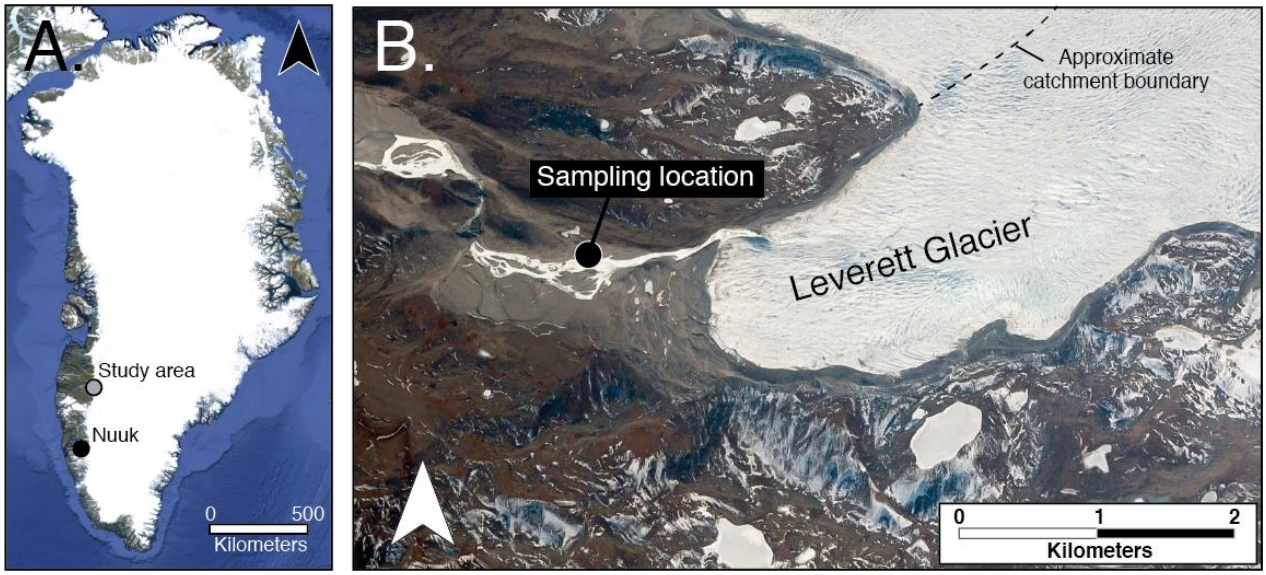


**Figure S-2** Map of Leverett Glacier, in the context of the Greenland Ice Sheet. **(a)** Landsat US Geological Survey, *via* Google), with the sample collection location shown by the black circle in **(b)** (DigitalGlobe, *via* Google), as published by Hawkings *et al.* (2018).

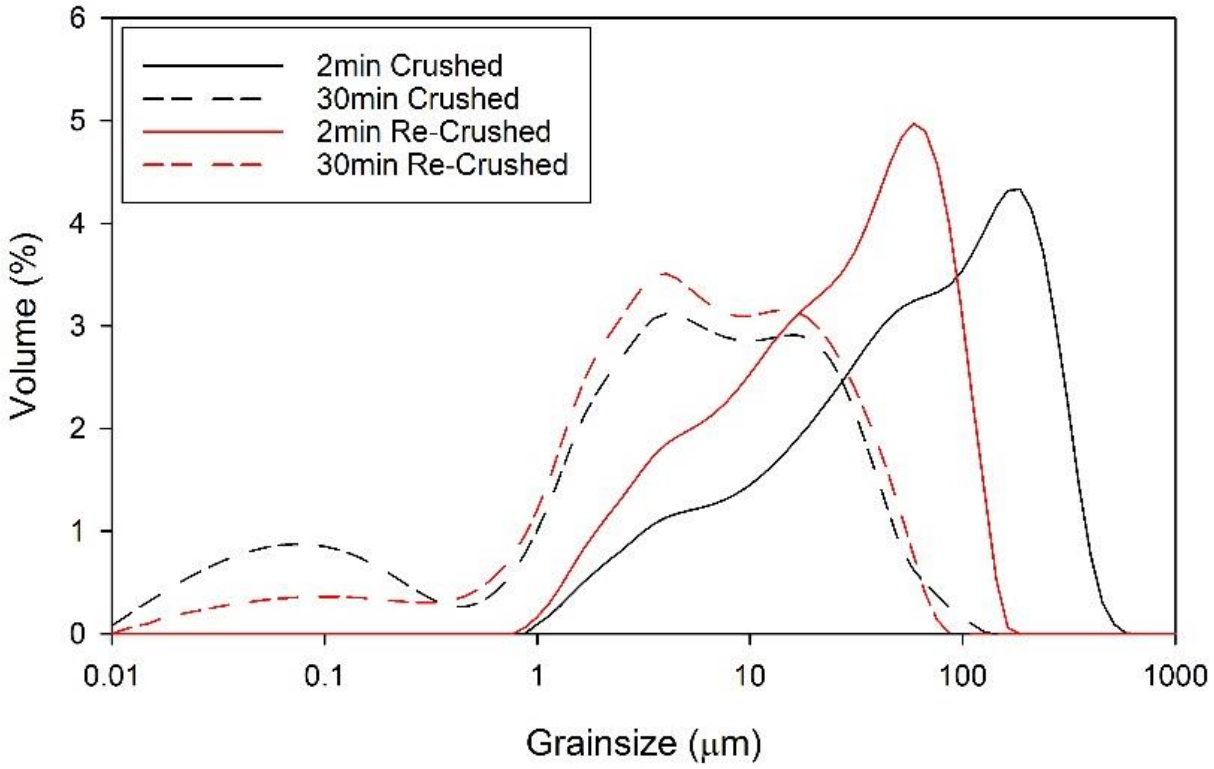


**Figure S-3** Grainsize distribution of T2 and T30 sediment, for primary and secondary crushing experiments. Black lines represent primary crushing experiments and red lines represent secondary crushing experiments, with solid lines showing T2 and dashed lines showing T30. Data is an average of 3 external replicate measurements, internally measured 5 times.

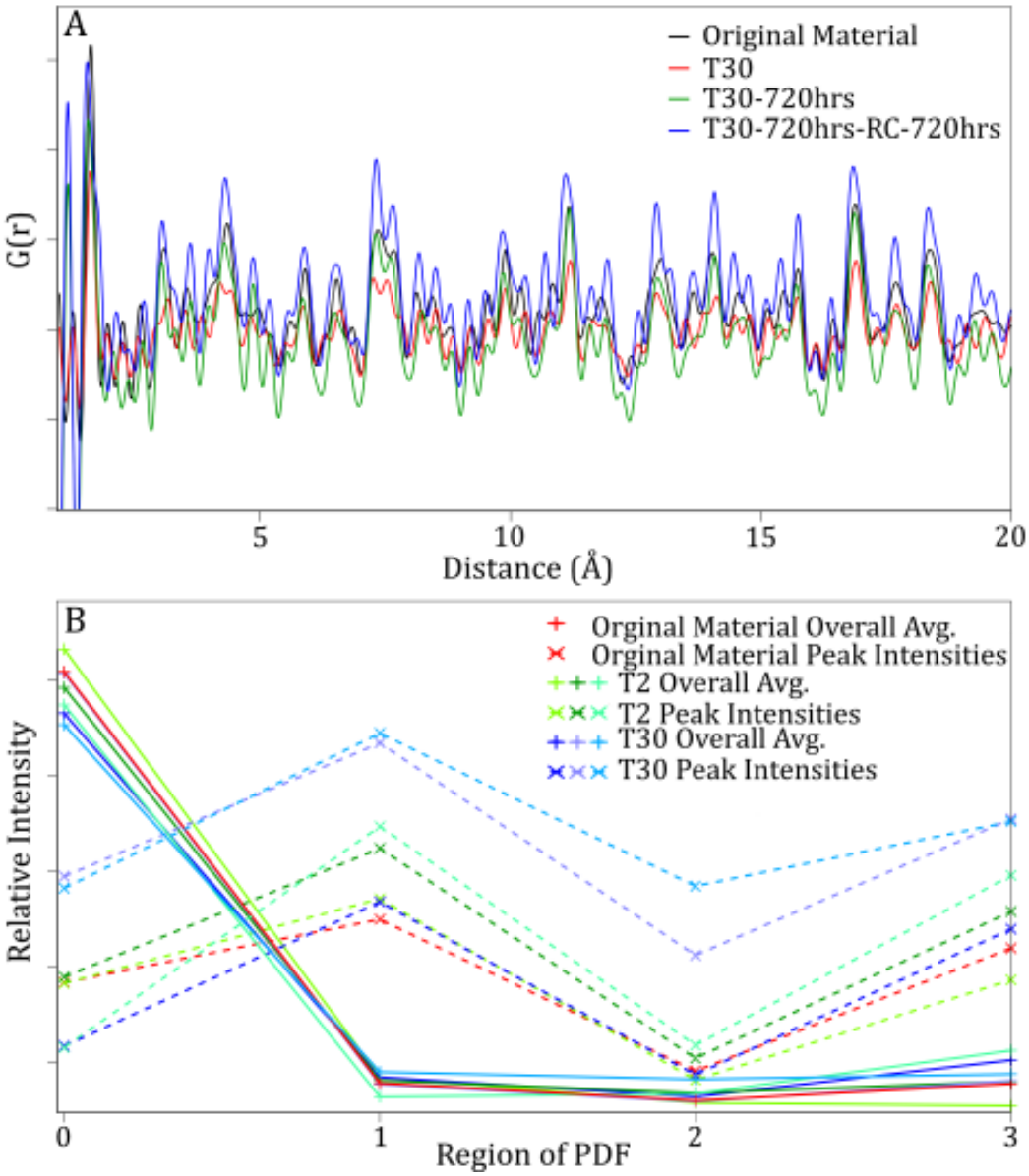


**Figure S-4** **(a)** Reduced pair distribution functions G(r) of samples T30 (milled and reacted) compared to the starting material before milling. **(b)** Plot of empirical crystallinity proxies. Solid lines (overall Avg.) correspond to integrated intensity under the PDF curve squared in 1st, 2nd, 3rd, 4th quarter of the PDF normalised by the maximum intensity of Si-O correlation peak (at 1.6Å). Dashed lines correspond to two highest peak intensity in each quarter sum normalised by the intensity of Si-O correlation peak. All samples follow the same crystallinity pattern, within error.

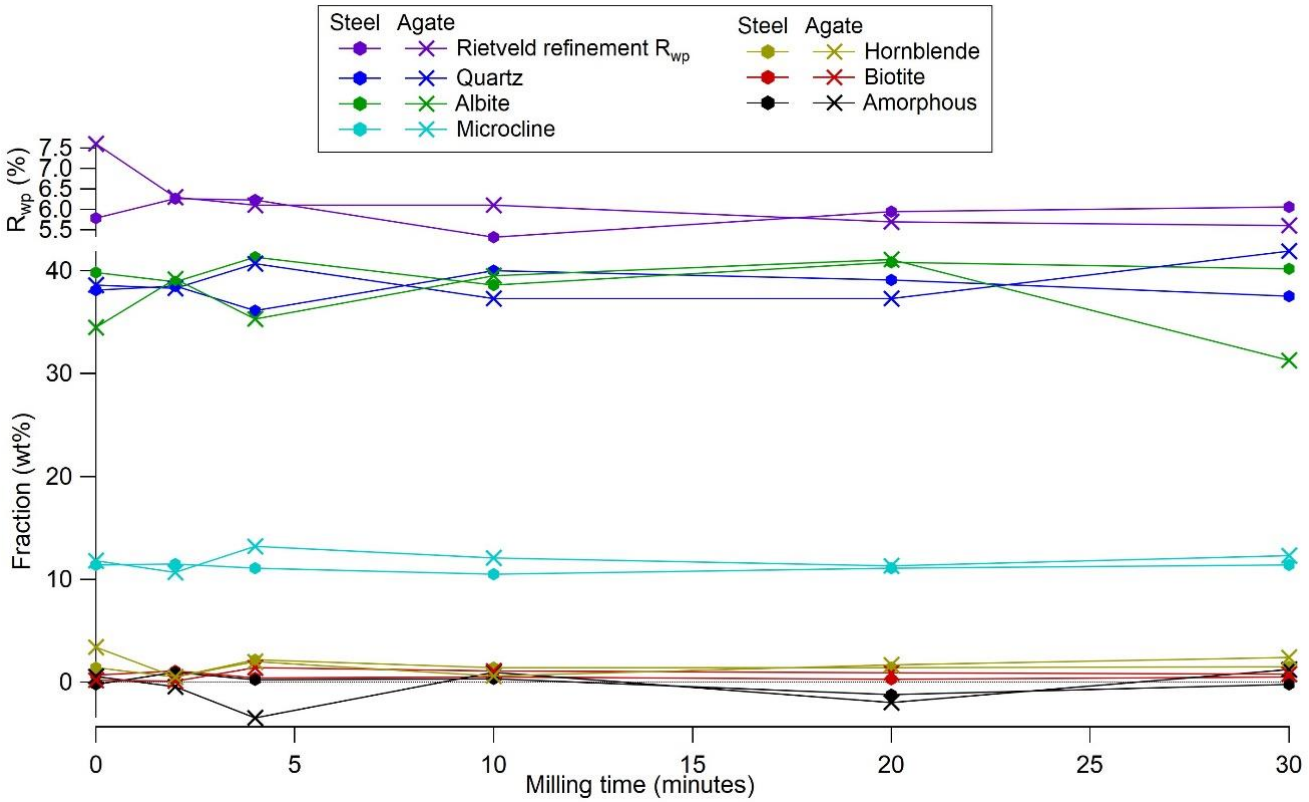


**Figure S-5** Mineralogical compositions of the samples milled with agate and steel mill for different duration of time. A slightly increased $R_{wp}$ of the agate milled t = 0 min sample is mostly likely caused by slightly coarser grain size (Fig. S-3) that has resulted in the sample measured not having completely uniform grain orientation averaging resulting in increased preferential orientation.

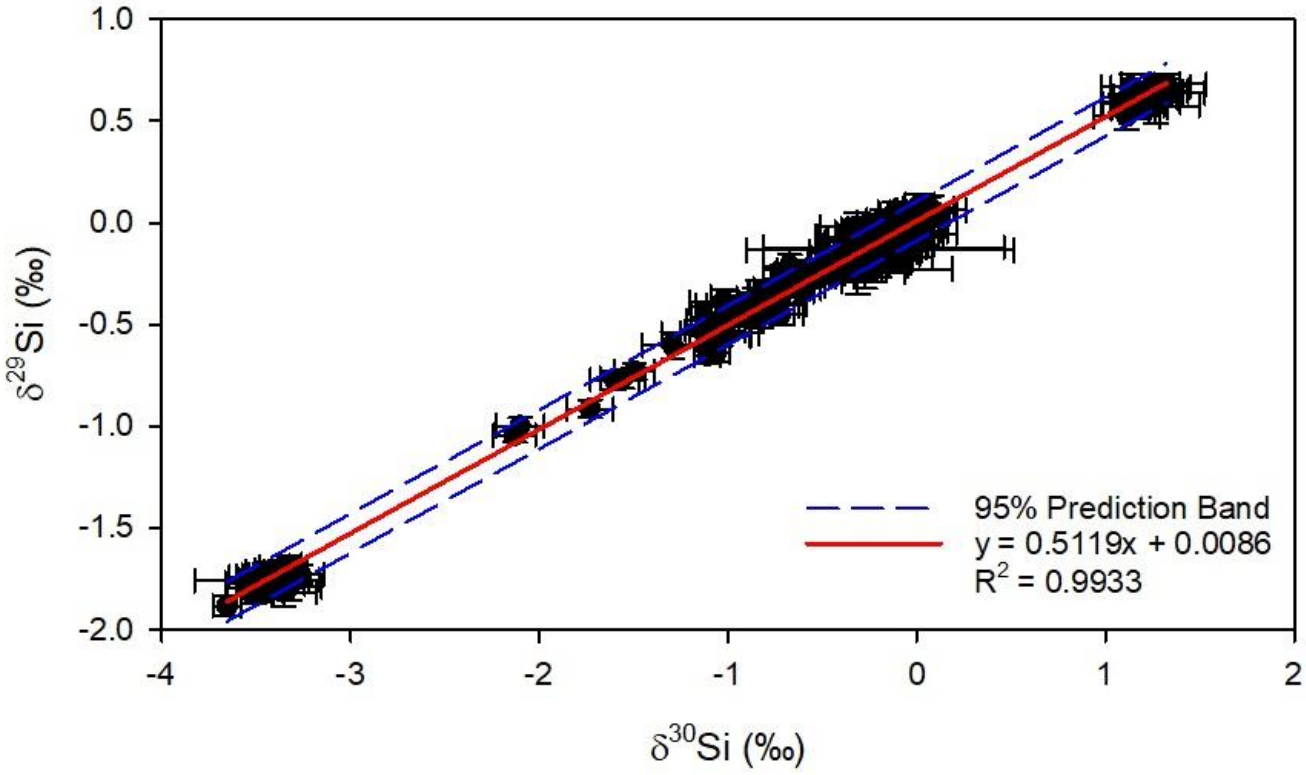


**Figure S-6** Three isotope plot of all measurements carried out during this study. Plot showing $\delta^{29}Si$ versus $\delta^{30}Si$ of samples and standards, with a red regression line of 0.512 ± 0.009 ‰. Blue dashed lines indicate the 95 % prediction intervals and error bars are the machine internal errors.

# Supplementary Information References

Bartholomew, I., Nienow, P., Sole, A., Mair, D., Cowton, T., Palmer, S., Wadham, J. (2011) Supraglacial forcing of subglacial drainage in the ablation zone of the Greenland ice sheet. *Geophysical Research Letters* 38, L08502.

Beaton, A.D., Wadham, J.L., Hawkings, J., Bagshaw, E.A., Lamarche-Gagnon, G., Mowlem, M.C., Tranter, M. (2017) High-Resolution in Situ Measurement of Nitrate in Runoff from the Greenland Ice Sheet. *Environmental Science & Technology* 51, 12518-12527.

Bouysse, P. (2014) *Geological Map of the World at 1:35 000 000*. Third Edition, CCGM-CGMW, Paris.

Cardinal, D., Gaillardet, J., Hughes, H.J., Opfergelt, S., André, L. (2010) Contrasting silicon isotope signatures in rivers from the Congo Basin and the specific behaviour of organic-rich waters. *Geophysical Research Letters* 37, L12403.

Clason, C.C., Mair, D.W.F., Nienow, P.W., Bartholomew, I.D., Sole, A., Palmer, S., Schwanghart, W. (2015) Modelling the transfer of supraglacial meltwater to the bed of Leverett Glacier, Southwest Greenland. *The Cryosphere* 9, 123-138.

Cowton, T., Nienow, P., Bartholomew, I., Sole, A., Mair, D. (2012) Rapid erosion beneath the Greenland ice sheet. *Geology* 40, 343-346.

DeMaster, J.D. (1981) The supply and accumulation of silica in the marine environment. *Geochimica et Cosmochimica Acta* 45, 1715-1732.

Egami, T., Billinge, S.J.L. (2003) *Underneath the Bragg Peaks*. First Edition, Pergamon, London.

Hatton, J.E., Hendry, K.R., Hawkings, J.R., Wadham, J.L., Kohler, T.J., Stibal, M., Beaton, A.D., Bagshaw, E.A., Telling, J. (2019) Investigation of subglacial weathering under the Greenland Ice Sheet using silicon isotopes. *Geochimica et Cosmochimica Acta* 247, 191-206.

Hawkings, J.R., Wadham, J.L., Tranter, M., Lawson, E., Sole, A., Cowton, T., Tedstone, A.J., Bartholomew, I., Nienow, P., Chandler, D., Telling, J. (2015) The effect of warming climate on nutrient and solute export from the Greenland Ice Sheet. *Geochemical Perspectives Letters* 1, 94-104.

Hawkings, J.R., Wadham, J.L., Benning, L.G., Hendry, K.R., Tranter, M., Tedstone, A., Nienow, P., Raiswell, R. (2017) Ice sheets as a missing source of silica to the polar oceans. *Nature Communications* 8, 14198.

Hawkings, J.R., Hatton, J.E., Hendry, K.R., de Souza, G.F., Wadham, J.L., Ivanovic, R., Kohler, T.J., Stibal, M., Beaton, A., Lamarche-Gagnon, G., Tedstone, A., Hain, M.P., Bagshaw, E., Pike, J., Tranter, M. (2018) The silicon cycle impacted by past ice sheets. *Nature Communications* 9, 3210.

Hendry, K.R., Leng, M.J., Robinson, L.F., Sloane, H.J., Blusztjan, J., Rickaby, R.E.M., Georg, R.B., Halliday, A.N. (2011) Silicon isotopes in Antarctic sponges: an interlaboratory comparison. *Antarctic Science* 23, 34-42.

Hindshaw, R.S., Rickli, J., Leuthold, J., Wadham, J., Bourdon, B. (2014) Identifying weathering sources and processes in an outlet glacier of the Greenland Ice Sheet using Ca and Sr isotope ratios. *Geochimica et Cosmochimica Acta* 145, 50-71.

Hughes, H.J., Delvigne, C., Korntheuer, M., de Jong, J., André, L., Cardinal, D. (2011) Controlling the mass bias introduced by anionic and organic matrices in silicon isotopic measurements by MC-ICP-MS. *Journal of Analytical Atomic Spectrometry* 26, 1892.

Kohler, T.J., Žárský, J.D., Yde, J.C., Lamarche-Gagnon, G., Hawkings, J.R., Tedstone, A.J., Wadham, J.L., Box, J.E., Beaton, A.D., Stibal, M. (2017) Carbon dating reveals a seasonal progression in the source of particulate organic carbon exported from the Greenland Ice Sheet. *Geophysical Research Letters* 44, 6209-6217.

Lawson, E.C., Wadham, J.L., Tranter, M., Stibal, M., Lis, G.P., Butler, C.E.H., Laybourn-Parry, J., Nienow, P., Chandler, D., Dewsbury, P. (2014) Greenland Ice Sheet exports labile organic carbon to the Arctic oceans. *Biogeosciences* 11, 4015-4028.

Qiu, X., Thompson, J.W., Billinge, S.J.L. (2004) PDFgetX2: a GUI-driven program to obtain the pair distribution function from X-ray powder diffraction data. *Journal of Applied Crystallography* 37, 678-678.

Reynolds, B.C., Aggarwal, J., Andre, L., Baxter, D., Beucher, C., Brzezinski, M.A., Engstrom, E., Georg, R.B., Land, M., Leng, M.J., Opfergelt, S., Rodushkin, I., Sloane, H.J., van den Boorn, S.H.J.M., Vroon, P.Z., Cardinal, D. (2007) An inter-laboratory comparison of Si isotope reference materials. *Journal of Analytical Atomic Spectrometry* 22, 561-568.

Savage, P.S., Georg, R.B., Williams, H.M., Burton, K.W., Halliday, A.N. (2011) Silicon isotope fractionation during magmatic differentiation. *Geochimica et Cosmochimica Acta* 75, 6124-6139.